Journal of Analytical and Applied Pyrolysis 176 (2023) 106241

Contents lists available at ScienceDirect

Journal of Analytical and Applied Pyrolysis

journal homepage: www.elsevier.com/locate/jaap

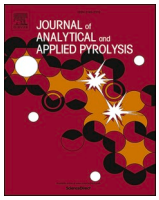

Fast pyrolysis of agricultural biomass in drop tube reactor for bio-oil production: Numerical calculations

Artur Bieniek *, Małgorzata Sieradzka, Wojciech Jerzak, Aneta Magdziarz

AGH University of Krakow, Mickiewicza 30 Av., 30-059 Cracow, Poland

ARTICLE INFO

Keywords:
Agricultural biomass
Fast pyrolysis
Computational fluid dynamics
Drop-tube reactor

ABSTRACT

Fast biomass pyrolysis is an effective method for bio-oil production and can be performed in fluidised beds, augers, and drop-tube reactors. In this study, the fast pyrolysis of agricultural biomass (oat and corn straw) in a drop-tube reactor was investigated by applying multiparameter analysis involving numerical calculations. The main motivation for this analysis was to determine the operating parameters for fast pyrolysis under which the highest bio-oil production was achieved. In this study, the following operating parameters were involved: pyrolysis temperature (500 – 700 °C), volume flow rate of the carrier gas (3 – 5 l/min), mass flow rate of the feedstock (10 – 30 g/h), and diameter of the particle (250 – 750 μm). The analysis was performed using numerical methods with the Euler-Lagrange multiphase theory in a 2D axisymmetric model. According to the numerical results, selection of a particle size of 500 μm, pyrolysis temperature of 500 °C, and nitrogen flow rate of 3 l/min allows obtaining 51.16% and 52.09% of bio-oil for oat straw and corn straw pyrolysis, respectively. The biomass mass load did not influence the final product yield. The numerical results were successfully confirmed by experimental investigations where experiments supplied 53.2% and 51.3% of bio-oil to oat straw and corn straw, respectively.

1. Introduction

Biomass pyrolysis is a promising process that involves organic materials such as wood, crop residues, and solid waste to produce green fuels such as bio-char, bio-oil, and gas [1]. This process is an important technology for replacing natural fossil fuels and for producing a wide range of valuable compounds for energy, chemical, and environmental purposes [2]. Biomass has recently gained increasing attention because of its potential for reducing greenhouse gas emissions and increasing the share of renewable energy in the primary energy demand [3].

Pyrolysis is a thermochemical process occurring at temperatures ranging from 400° to 800°C in the absence [2] or minor presence of oxygen [4]. Biomass pyrolysis products include bio-char (a solid product remaining after the process), bio-oil (heavy hydrocarbons included in volatile matter), and gas (lightweight gases) [5]. The feedstock is rapidly heated and undergoes chemical and physical conversions, releasing volatile matter [5]. Pyrolysis can be classified into three main types: slow, intermediate, and fast. This study focused on fast pyrolysis, which involves temperatures of approximately 500 °C, heating rates ranging above 10 – 200 °C/s, and biomass residence times up to few seconds [6]. Fast pyrolysis results in high bio-oil yield, which is the most desirable product of this process [7].

Pyrolysis can be conducted in various reactors. There are several types of reactors, including fixed-bed, fluidised, drop-tube, and auger reactors [8]. The drop-tube reactor is suitable for pyrolysis; it is characterised by low residence time and high heating rate and provides a large amount of bio-oil [9]. According to the literature review, the fixed-bed reactor seems to be the most universal reactor, where the number of observations recorded in the literature review is approximately 1610 [10].

This study focused on fast pyrolysis, which leads to the production of bio-oil. Therefore, the reactor should be capable of producing a high yield of liquid products. These criteria can be fulfilled using a drop-tube reactor, also known as an entrained-flow reactor. A high bio-oil yield from wood pyrolysis in a drop-tube reactor was confirmed by Guizani et al. [11]. The bio-oil yield was 62.4% at 500 °C with a particle size of 370 μm. Particle size and temperature had the highest impact on bio-oil yield. Ellens and Brown [12] also confirmed a high amount of bio-oil at a level of 71.1% during pyrolysis of red oak at 550 °C. Despite high bio-oil yields, there are some challenges that have a negative impact on biomass pyrolysis in a drop-tube reactor and reduce bio-oil content. The large

* Corresponding author.
E-mail address: artbie@agh.edu.pl (A. Bieniek).

https://doi.org/10.1016/j.jaap.2023.106241
Received 31 May 2023; Received in revised form 25 August 2023; Accepted 29 October 2023
Available online 2 November 2023

Nomenclature

A	surface, m^2.
A_r	preexponential factor, s^{-1}.
a	heat transfer coefficient, W m^{-2} K^{-1}.
a_1, a_2, a_3	constants for drag force coefficient determination.
Bi	Biot number, (-).
C_D	drag force coefficient, (-).
C_1	mean reacting gas species concentration at the particle surface, kg m^{-3}.
$C_{j,r}$	molar concentration of species j in reaction r, kg mol m^{-3}.
d	diameter, m.
D_0	diffusion rate for particle surface reaction, (-).
D_m	coefficient of mass diffusivity, m^2 s^{-1}.
D_T	coefficient of thermal diffusivity, m^2 s^{-1}.
e	emissivity, (-).
E	internal energy, J.
E_a	activation energy, kJ mol^{-1}.
F	force, N.
g	gravity force, m s^{-2}.
h	specific enthalpy, J kg^{-1}.
H	enthalpy, J.
DPM	discrete phase model.
i	i_{th} species.
j	j_{th} reaction.
kin	kinetic.
n	bulk.
α	volume fraction, (-).
η	effectiveness factor, (-).
μ	dynamic viscosity, Pa s.
k_r	rate of reaction, s^{-1}.
j	mass diffusivity, kg $m^{-2}s^{-1}$.
k	thermal conductivity, W $m^{-1}K^{-1}$.
M	molar mass, g mol^{-1}.
n	reaction order, (-).
Nu	Nusselt's number.
p	pressure, Pa.
Pr	Prandtl's number, (-).
R	gas constant, J $K^{-1}mol^{-1}$.
$\mathscr{R}$	mass source due to homogenous reaction, mol s^{-1}.
$\overline{R}$	rate of particle surface reaction, kg s^{-1}.
R_{kin}	rate of particle surface reaction per unit area, kg $m^{-2}s^{-1}$.
Re	Reynold's number, (-).
S	source term.
S_{rn}	radiation source energy, W m^{-3}.
t	time, s.
T	temperature, K.
v	velocity vector, m s^{-1}.
Y	local concertation, (-).

Subscript

p	particle.
r	r_{th} reaction.
rn	radiation.
s	solid.
∞	ambient.

Greek letter

ρ	density, kg m^{-3}.
σ	Stefan – Boltzmann constant, W m^{-2} K^{-4}.
τ	stress tensor, Pa.

diameter of the reactor causes a temperature gradient in the axial direction, which impacts the non-uniform heating of biomass particles that do not fully convert. This problem was the subject of a study investigated by Bieniek et al. [13], who proposed the addition of oxygen to partially oxidise the evolved char and shift the evolution of the products toward gaseous species. Gable and Brown [14] determined the heating time of particles inside the reactor. The paper presented that at a heating time of 1.4 s; a lot of unreacted biomass remained, and the solid residue consisted of approximately 56% pyrolytic products. Another problem is the variety of operating conditions of the reactor as well as the complex composition of various biomasses [15,16]. There are no universally used parameters for all types of biomass because of the different cellulose, hemicellulose, and lignin contents. Each basic component was responsible for bio-oil production in a different way. Cellulose has the greatest impact on bio-oil production, whereas lignin is the main contributor [17,18]. Additionally, lignin has the highest temperature of thermal conversion at approximately 400 °C [19]. Considering the presented challenges, it is necessary to determine the operating conditions for the considered biomass to provide high pyrolysis efficiency, especially for bio-oil production.

Operating parameters can be established in two ways. The first involves experimental studies that lead to the attainment of expected values. However, this method is expensive, time consuming, and requires laboratory resources. The second method involves theoretical studies including CFD (computational fluid dynamics) calculations. This method allows the determination of operating parameters based on the governing equations for the conservation of mass, energy, and species. This process involves the use of mathematical models and computational simulations to predict the behaviour of the biomass feedstock during pyrolysis and the yield and composition of the resulting products. Because biomass pyrolysis is a multiphase flow, two approaches to the multiphase theory can be applied: Euler – Euler (both phases are treated as interpenetrated fluids) and Euler – Lagrange (the solid phase is dispersed in the fluid phase and is described by Newton's laws). A detailed comparison of these two models can be found in study [2]. Xue et al. [20] used the Euler – Euler model to determine the operating parameters of the fast pyrolysis of red oak in a fluidised bed reactor. The results indicated that the temperature, gas flow rate, and particle size were mainly responsible for bio-oil production. Aramideh et al. [21] studied the pyrolysis of red oaks using an auger reactor. A numerical model with an Euler – Euler approach allowed to find the temperature of 550 °C as the best option for bio-oil production. In another study, Xue et al. determined the product yield of bagasse pyrolysis in a fluidised bed reactor at 790 K [22]. CFD calculations allowed the estimation of approximately 63.4% bio-oil. Kong et al. applied the Euler – Lagrange theory to investigate biomass pyrolysis in a V-shaped reactor, where the ratio of the carrier gas flow rate to the mass flow rate of biomass was investigated [23]. The researchers discovered that a 20:1 ratio was the best option for providing the most effective heat transfer between the fluid and solid phases. Numerical calculations of biomass pyrolysis in drop-tube reactors using the Euler – Euler approach were conducted by Tobo et al. [24], who investigated the yields of products and their characterisation.

This study concerns multiparameter analysis of fast pyrolysis in a drop-tube reactor that involves numerical methods using the Euler – Lagrange multiphase theory. The main motivation of this study was to determine the process parameters that allow maximum bio-oil production. Biomass pyrolysis is a complex process influenced by interconnected parameters, including reactor type and performance. Conducting a multiparameter analysis allows the identification of the best parameters to achieve the desired goal. Moreover, owing to multiparameter analysis, it is possible to understand the behaviour of

biomass particles during pyrolysis. In particular, numerical calculations can be helpful because of the possibility of determining distributions such as the temperature and yield of products.

According to state-of-the-art methods, multiparameter analysis mainly concerns fixed-bed and fluidised bed reactors. There is a lack of studies, especially numerical investigations, on drop-tube reactors. Therefore, this study will be of special interest to readers in the following fields:

i) Development of a numerical model of fast pyrolysis in a drop-tube using the Euler-Lagrange multiphase theory.

ii) Investigate the influence of operating parameters on feedstock properties and reactor performance in bio-oil production.

iii) Understanding particle behaviours during fast pyrolysis under various conditions.

iv) Selection of the best parameters for bio-oil production based on the numerical results and their verification via experimental investigations.

Furthermore, the proposed numerical model can be helpful for determining the operating parameters of various feedstocks. The advantage of this strategy is that each parameter is separately tested without involving experiments, which can save material and financial resources.

2. Materials and methods

2.1. Feedstock characterization

In this study, two lignocellulosic biomasses were selected from agricultural sources in Poland: oats and corn straw. These biomasses are the harvested residues. The materials selected for laboratory pyrolysis experiments were initially dried at room temperature and then ground in a mill. Basic analyses were then performed, including ultimate, proximate, and fibre analyses. The Truspec CHNS 628 Leco analyser was involved in the ultimate analysis. Proximate analyses were performed according to the following standards: EN ISO 18134–2:2017 (moisture), EN ISO 18122:2015 (volatile matter), and EN ISO 18122:2015 (ash). The fibre analysis was performed according to the van Soest method [25], where cellulose, hemicellulose, lignin, and extractive contents were determined. All basic analyses were performed at least three times, and the average value was calculated. The results of all the analyses are presented in Table 1.

2.2. Experimental setup

The drop-tube reactor presented schematically in Fig. 1a) is an electrically heated furnace that includes a reactor tube, micro feeder, char container, and bio-oil condensation unit. A microfeeder was installed at top of the reactor. Biomass was loaded inside the reactor at mass flow rates of 10, 20, or 30 g/h. The fallout of biomass particles was enhanced by nitrogen flow. Nitrogen was supplied at a flow rate of 3 – 5 l/min using a microfeeder connected to a rotameter. A water jacket was installed under the microfeeder to prevent biomass from heating prior to reaching the heating zone. The stainless-steel reactor tube has a heated zone with a length of 2 m and an inner diameter of 0.015 m. The temperature along the length of the reactor was monitored using five K-type thermocouples spaced every 0.5 m. Bio-char particles were collected at the end of the pyrolysis experiment using a stack impactor. The bio-oil was then condensed in an ice-filled bucket. The bio-char and bio-oil yields were determined by weighing the pyrolysis products.

2.3. Numerical model of drop-tube reactor

This study presents a 2D numerical analysis of the fast pyrolysis of oat straw and corn straw in a drop-tube reactor. The model was prepared based on the previously mentioned laboratory setup and is presented in Fig. 1b).

The proposed model comprised two zones. The first zone was the heating area with a total length L of 2 m. Before heating the zone, 0.2 m of nonheated area was added. This allowed for the development of the velocity distribution of the carrier gas. The total length of the first zone in this area L_r was 2.2 m. The second zone was the cooling area. This zone did not have a physical representation but was added to maintain the stability of the calculation and prevent backflow to the reactor. The cooling zone was 1 m long. The diameter of the reactor d was 0.015 m.

At the top of the reactor, the velocity inlet boundary condition was set with a uniform nitrogen velocity appropriate for the investigated carrier gas flow rate parameters. The temperature of the inlet gas was 25 °C. In this study, laminar flow was considered and a subgrid turbulence model was not included. A uniform surface mass load of the biomass was applied at the inlet. The mass flow rate of the particles was one of the parameters studied. Spherical particles were also considered. The particle diameter was variable and referred to as the investigated particle size. Under actual conditions, biomass particles are characterised by irregular shapes. Therefore, treating biomass particles as spheres can limit the following quantities: drag force, heat and mass force, and particle–wall interactions. However, such simplifications allow for the implementation of well-known models for heat and mass transfer. Isothermal boundary conditions were established in the reactor-heating zone. The temperature was related to the investigated pyrolysis temperature parameters. In the rest of the numerical model, on the wall, a convective-radiative thermal boundary condition was applied with an ambient temperature of 25 °C and a heat transfer coefficient of 10 W/m^2K [26]. On the outlet surface, the pressure-outlet boundary condition was established with a surrounding pressure of 101325 Pa at 25 °C. The transient calculations were performed using the initial temperature inside the heating zone related to the investigated temperature parameters. The model was placed in a cylindrical framework and an axial boundary condition was applied in the middle of the model. However, it is noteworthy that, in reality, there is no symmetry in the pyrolysis process. However, the axis boundary simplifies the model to a 2D analysis by reducing the number of mesh elements and computation time. Furthermore, there were no significant differences in the product yields between the 2D and 3D systems after preliminary studies.

2.4. Mathematical model

The Euler – Lagrange multiphase theory was used in this study. This

Table 1
Ultimate, proximate, and fiber analyses of oat straw and corn straw at an air-dry state ([a]O = 100% – C – H – N – A; [b]FC = 100% – M – VM – A; [c]Extractives = 100% – Cellulose – Hemicellulose – Lignin – M – A).

Sample	C wt%	H wt%	N wt%	O[a] wt%	M wt%	VM wt%	A wt%	FC[b] wt%
Oat straw	44.11	5.98	0.62	43.65	6.03	76.90	5.64	11.43
Corn straw	43.12	6.19	1.44	35.68	9.23	62.82	13.57	14.39
Sample	**Cellulose wt%**		**Hemicellulose wt%**		**Lignin wt%**		**Extractives[c] wt%**	
Oat straw	41.07		24.62		5.16		17.48	
Corn straw	32.76		29.08		2.81		12.55	

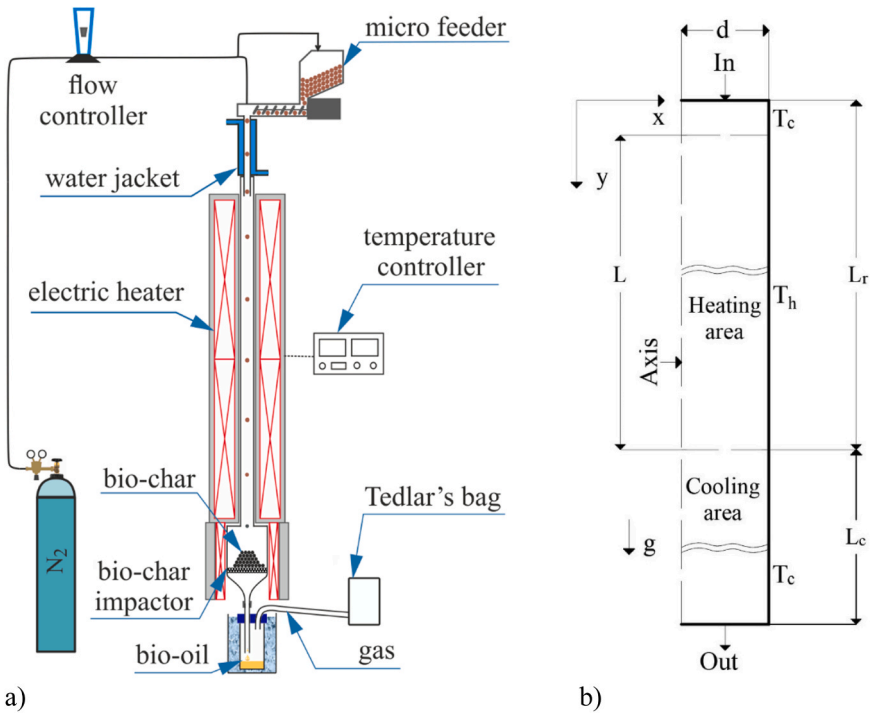

Fig. 1. a) Scheme of laboratory set-up and b) numerical model of the drop-tube reactor.

approach assumes that biomass particles are discrete phases that move in the fluid zone, which is a mixture of the volatiles (generated during pyrolysis) and the carrier gas. The principle of this model is to not exceed the volume fraction of solid particles by more than 12%, even if the mass ratio of solid to gas is much higher. Therefore, biomass particles should fill up to 12% of cell size. Biomass particles are highly dispersed in the drop-tube reactor; thus, this model can be successfully applied, and the above mentioned limitations can be fulfilled. Additionally, the Euler – Lagrange model allows the tracking of every particle or parcel of particles, and their behaviours can be monitored with very good results [23, 27].

The following set of equations were solved for the Eulerian and Lagrangian phases which refer to the conservation of mass, momentum, heat, and species. The general equations for the Eulerian phase are presented in Table 2:

The terms S_{DPM} and $\vec{F}_{DPM}$ refer to the mass, heat, species, and momentum added to the continuous phase as a result of the interaction of fluid solids. A detailed explanation of the calculations of these sources is presented in [28]. In Eq. (6), two mass-transfer sources are considered. The first source refers to the differences in mass concentration (Fick's law). The second source involves mass transfer owing to the temperature gradient (Soret's law).

The general equations for the Lagrangian phase are listed in Table 3. The calculation of the drag force coefficient involved the Reynolds number and three constants provided by Morsi and Alexander [29]. Eq. (9) represents the formula used. This equation is suitable for spherical particles. The experimental equations developed by Ranz and Marshal are shown in Eq. (13) and were used to determine the heat transfer coefficient [30]. The advantages of this correlation include easy implementation and applicability to forced convection during laminar flows.

Table 2
Set of equations for Eulerian phase.

Name	Equation	No.
Mass conservation of the fluid phase	$\frac{\partial \rho}{\partial t} + \nabla(\rho \vec{v}) = S_{DPM} + S_{other}$	(1)
Conservation of momentum of the fluid phase	$\frac{\partial(\rho \bullet \vec{v})}{\partial t} + \nabla(\rho \vec{v} \vec{v}) = -\nabla p + \nabla \tau + \rho \vec{g} + \vec{F}_{DPM} + \vec{F}_{other}$	(2)
Stress tensor τ	$\tau = \mu\left[\left(\nabla \vec{v} + \nabla \vec{v}^{T}\right) - \frac{2}{3}\nabla \vec{v} I\right]$	(3)
Conservation equation of the energy of fluid phase	$\frac{\partial(\rho \bullet E)}{\partial t} + \nabla(\vec{v}(\rho E + p)) = \nabla\left(k\nabla T - \sum_i h_i \vec{J}_i + (\tau \vec{v})\right) + S_{DPM} + S_{rn} + S_{other}$	(4)
Species transport equations	$\frac{\partial(\rho \bullet Y_i)}{\partial t} + \nabla(\rho \vec{v} Y_i) = -\nabla \vec{J}_i + \mathscr{R}_i + S_{DPM,i} + S_{other,i}$	(5)
Diffusion flux $\vec{J}_i$ of i_{th} species in fluid phase	$\vec{J}_i = -\rho D_{m,i} \nabla Y_i - D_{T,i} \frac{\nabla T}{T}$	(6)

Table 3
Set of equations for Lagrangian phase.

Name	Equation	No.
Balance of forces of solid phase	$\frac{d\vec{v}_p}{dt} = F_D(\vec{v} - \vec{v}_p) + \frac{\vec{g}(\rho_p - \rho)}{\rho_p} + \vec{F}_x + \vec{F}$	(7)
Drag force F_D	$F_D = \frac{18\mu C_D Re_s}{24\rho_p d_p^2}$	(8)
Drag coefficient for smooth particles	$C_D = a_1 + \frac{a_2}{Re_s} + \frac{a_3}{{Re_s}^2}$	(9)
Reynold's number of solid phase	$Re_s \equiv \rho d_p \left\lvert \frac{\vec{v}_p - \vec{v}}{\mu} \right\rvert$	(10)
$\vec{F}_x$ the virtual mass force	$\vec{F}_x = 0.5 \frac{\rho}{\rho_p} \frac{d}{dt}(\vec{v} - \vec{v}_p)$	(11)
General formula of heat balance of a solid particle	$m_p c_p \frac{dT_p}{dt} = aA_p(T_\infty - T_p) + e_p A_p \sigma\left(T^4 - T_p^4\right) - \frac{dm_p}{dt} H_{reaction}$	(12)
Heat transfer coefficient	$Nu = \frac{ad_p}{k_\infty} = 2 + 0.6 Re_s^{\frac{1}{2}} Pr^{\frac{1}{3}}$	(13)
Mass of single solid particle	$m_p = \sum_{i=1}^{n} Y_i \rho_i \frac{4\pi d_p^3}{3}$	(14)
Conversion rate of particle	$\frac{dm_p}{dt} = -m_p \sum_j^n \overline{R}_{j,r}$	(15)

2.5. Reaction kinetic and material properties

Fig. S1 (Supplementary Material) illustrates the pyrolysis reaction mechanism used in the calculations. The pyrolysis mechanism is based on a study by Miller and Bellan [17]. Researchers have proposed a comprehensive mechanism for pyrolysis involving primary and secondary reactions. This mechanism assumes that the biomass is composed of three main components: cellulose, hemicellulose, and lignin. Each component reacts separately, making this mechanism comprehensive and involving numerous individual reactions. During the analysis, bio-oil and gas compositions were not considered. Therefore, the proposed reaction mechanism offers computational advantages owing to its easy implementation and less time consumption. Additionally, it is a valuable tool for predicting the product yields under different pyrolysis conditions. According to this mechanism, the pyrolytic products are classified into three main groups: char (solid residues, including ash), liquid (primary tars and moisture), and lightweight gases (pyrolytic gas, CO, CO_2, etc.). The thermal conversion reactions of the biomass were computed according to the particle surface reactions, and the equations are presented in Table 4.

All the reactions considered in this study are presented in Table S1 (Supplementary Materials). Furthermore, in Table S2, all kinetic data applied in the calculation are presented with respect to the values proposed by Miller and Bellan [17].

The physical and chemical properties of the Eulerian and Lagrangian phases used in this study are listed in Table S3 (Supplementary Material). The following assumptions were made to simplify the calculations: a) biomass was built with three main components with respect to fibre analysis from Table 1; b) extractives were treated as hemicellulose, according to a previous study [17]; c) active components had the same properties as raw components; d) thermal diffusivity coefficient D_T and mass diffusivity coefficient D_m were estimated according to the kinetic theory proposed by [31]. These values were obtained using ANSYS Fluent software [28].

2.6. Analysed operating parameters

The operating parameters of the drop-tube reactor depend on the design and objectives of the pyrolysis process. Four parameters were considered and their values are listed in Table 5.

Multiparameter analysis was conducted as follows. First, the reference operating conditions were determined based on the reactor geometry and performance. The reference conditions involved were a particle size of 500 μm, inert gas flow rate of 3 l/min, biomass mass load of 20 g/h, and temperature of 500 °C. During the analysis, for example, only the diameter of the particle was changed for the particle size. After investigating all particle size values, the operating conditions returned to the reference values and moved to the next category of parameters. This procedure was repeated for all the four categories.

Table 4
Set of equations for particle surface reactions.

Name	Equation	No.
Thermal conversion reactions of biomass	$\overline{R}_{j,r} = A_p \eta_r Y_j R_{j,r}$	(16)
Term $R_{j,r}$ was computed	$R_{j,r} = R_{kin,r}(p_n - \frac{R_{j,r}}{D_{0,r}})^N$	(17)
Coefficient of diffusion rate	$D_{0,r} = C_{1,r}\frac{(\frac{T_p + T_\infty}{2})^2}{d_p}$	(18)
Kinetic rate of reaction by Arrhenius theory	$R_{kin,r} = A_r e^{-\frac{E_a}{RT}}$	(19)
Homogenous reaction rate of thermal cracking	$\mathscr{R}_{i,r} = M_i R_{kin,r} \prod_{j=1}^{k} [C_{j,r}]^N$	(20)

Table 5
Analysed operating parameters of fast pyrolysis.

Parameter	Symbol	Values
Particle size	d_p,	250, 500, and 750 μm
Inert gas flow rate	V_f,	3, 4, and 5 l/min
Biomass mass load	m_p,	10, 20, and 30 g/h
Temperature	T_r,	500, 600, and 700 °C

2.7. Calculation methodology and model sensitivity test

Transient numerical calculations of the fast pyrolysis of agricultural biomass were performed using ANSYS Fluent 2022R1 software. Euler – Lagrange multiphase approach, known as the discrete phase model (DPM), was used in Fluent software. During the calculations, a two-way coupling effect was involved in which the discrete phase also influenced the fluid phase owing to mass, momentum, and heat exchange. Increasing the particle size increases the importance of the interaction between the fluid and solid. DPM can successfully capture these interactions until suitable conditions are ensured. The main limitation of this model is that the volume fraction of the solid phase in the cell should not exceed 0.12. This concerns the global domain and local zones where particles can accumulate during flow. The aforementioned assumptions favour meshes with high element sizes. The model sensitivity tests involved four uniform meshes with quadrilateral elements, different dimensions, and different numbers of elements. In addition, four time steps were tested to reduce the computation time and preserve the accuracy of the results.

Mesh I consisted of elements 1 × 3 mm in size, with a total amount of 8 712. Mesh II had 16 110 elements with 0.75 × 2 mm in size. Mesh III was built with 35 565 elements of 0.5 × 1.5 mm in size. Mesh IV contained 64280 elements that were 0.375 × 1 mm in size. The element size was selected based on studies [22,32]. Time-step analysis considered the following time steps: 5×10^{-4} (adjusted to the fastest reaction), 1×10^{-3}, 2×10^{-3} and 5×10^{-3} seconds.

All mathematical equations were solved in a cylindrical framework, and the following discretisation schemes were used. A simple discretisation scheme was set for the velocity – pressure field. A second-order upwind scheme was used for the equations concerning the conservation of mass, energy, momentum, and species. The convergence criteria were set to 1×10^{-4} for all equations. The maximum number of iterations was set to 20. The source terms of the fluid phase were updated every three iterations.

Model sensitivity tests were performed on oat straw. The reference operating parameters of the drop-tube reactor were considered as input data. The impact of the mesh size was calculated with a time step of 1×10^{-3} s. Time-step analysis involved mesh II. The mass flow rate of the bio-oil was monitored at the reactor outlet. The results of these tests are shown in Fig. 2.

According to the presented results, the mesh size and time step had no impact on the bio-oil yield. All curves almost overlapped and exhibited the same tendency. Fig. 2 shows that 5 s were required to stabilise the flow, after which a pseudo-steady condition was observed. The lack of noticeable differences allows one to involve a large cell size and time step, which decreases the computation time. For further analysis, Mesh II with 16110 elements and a time step of 2×10^{-3} s was selected.

3. Results of numerical calculations

3.1. Impact of particle size

Fig. 3 shows the numerical results of the pyrolysis product yields as a function of the studied biomass particle size. The products were classified into three groups: bio-char (solid residue after pyrolysis), bio-oil (condensable matter of pyrolytic vapour, including water), and gas

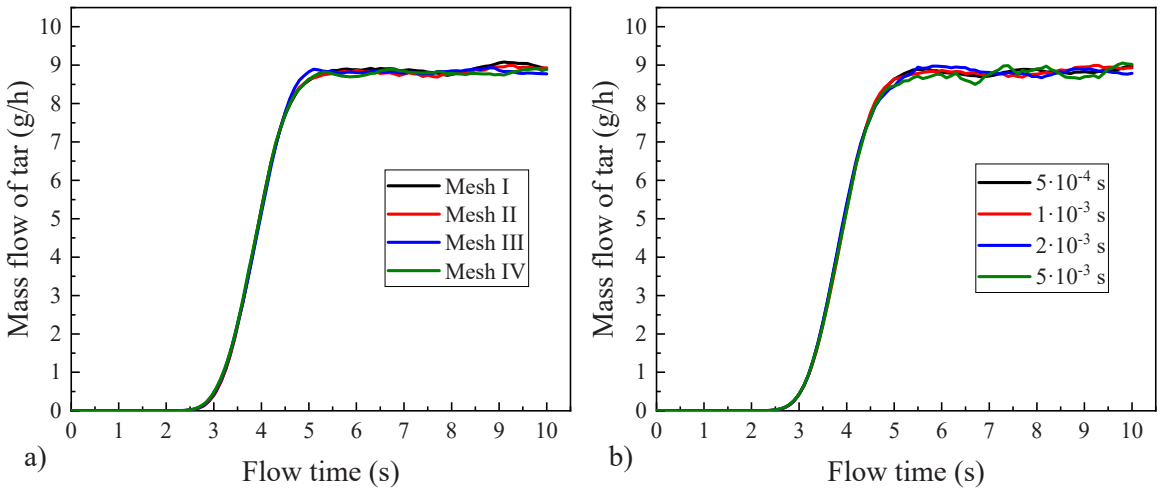

Fig. 2. Results of model sensitivity tests for a) mesh impact and b) time step impact.

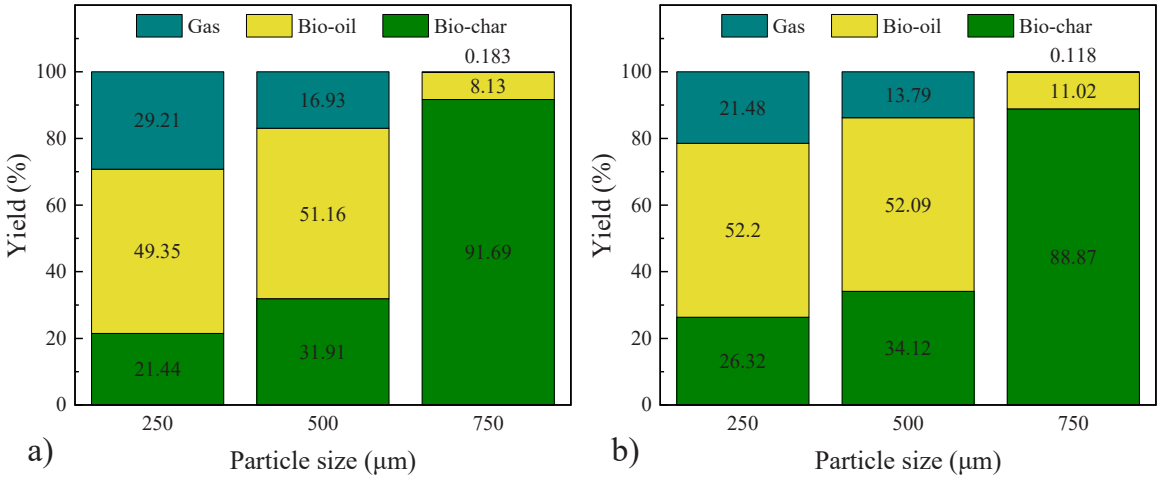

Fig. 3. Numerical results of product yields of fast pyrolysis of a) oat straw and b) corn straw as a function of biomass particle size.

(lightweight gases).

The numerical results showed a significant influence of particle size on the pyrolytic product concentration. For both feedstocks, the particle size of 250 μm favours high condensed matter content of approximately 50%, which is a promising result in the case of bio-oil production. Moreover, only a small amount of bio-char was generated at this particle size. This means that a large part of the biomass was converted into pyrolytic vapour and 29.21% and 21.48% of gas was generated for oat straw and corn straw, respectively. At a particle size of 500 μm, a large amount of bio-oil was also produced with a particle size of oat straw pyrolysis. This particle size provided the highest bio-oil concentration. However, more bio-char was obtained, which can be explained more uncreated components remaining in the particles. Additionally, the higher the particle size, the lower the gas yield.

The size of the biomass particle of 750 μm gave negative results in bio-oil production. Approximately 90% of bio-char and approximately 10% of oil were received under these conditions. The amount of oil was correlated to the moisture content of biomass. This implies that this particle size provides only moisture evaporation and the particles do not start pyrolysis. To better understand the behaviour of the biomass particles in a drop-tube reactor, the particle conversion rate distribution for both feedstocks is presented in Fig. 4. The presented distributions were zoomed 15 times in the radial direction for better visualisation owing to the high length-to-diameter ratio.

Fig. 4 shows the areas where biomass pyrolysis occurred with varying particle sizes. It can be observed that the smaller the particle size, the shorter the reactor length. This observation is important for determining the reactor geometry and optimising its length at a specific temperature. Fig. 4 shows the negative effect of a particle size of 750 μm on biomass pyrolysis. Only a small conversion rate was observed at the centre of the reactor, which was related to moisture evaporation. To improve the pyrolysis using this particle size, it is necessary to extend the reactor length or increase its temperature.

The explanation of the presented results is related to the particle heating rate and residence time. The rearranged form of Eq. (12) was used to determine the heating rate and $\frac{dT_p}{dt}$ was calculated. Fig. 5 shows the results of the calculations of the aforementioned parameters.

From the presented Fig. 5a), it can be observed that the particle size impacted residence time. The smallest particles remained in the heating zone for approximately 2.5 s. Increasing the particle size nonlinearly shortened the residence time by up to approximately 0.9 s. This was related to the particle terminal velocity. Generally, two main forces act on a solid body dropping in the fluid domain: gravity and drag force (dependent on velocity). Initially, gravity dominates the drag force and the solids move with acceleration until both forces become equal. The body then undergoes a uniform rectilinear motion with a velocity equal to the terminal velocity, which is related to the mass and surface area of the particle [33].

Fig. 5b) shows that the particle size also affects the heating rate. At a

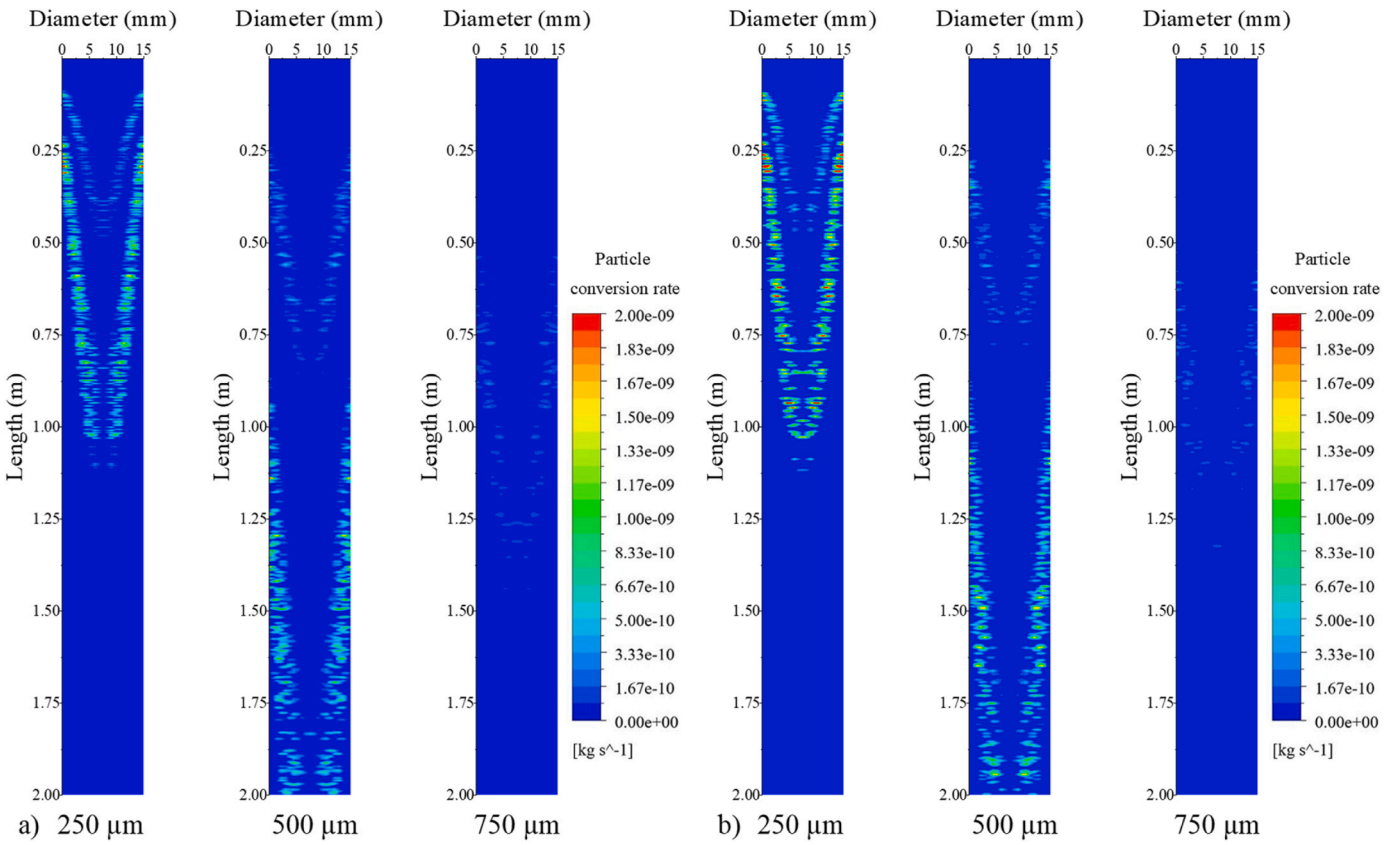

Fig. 4. Distribution of particle conversion rate for pyrolysis of a) oat straw and b) corn straw.

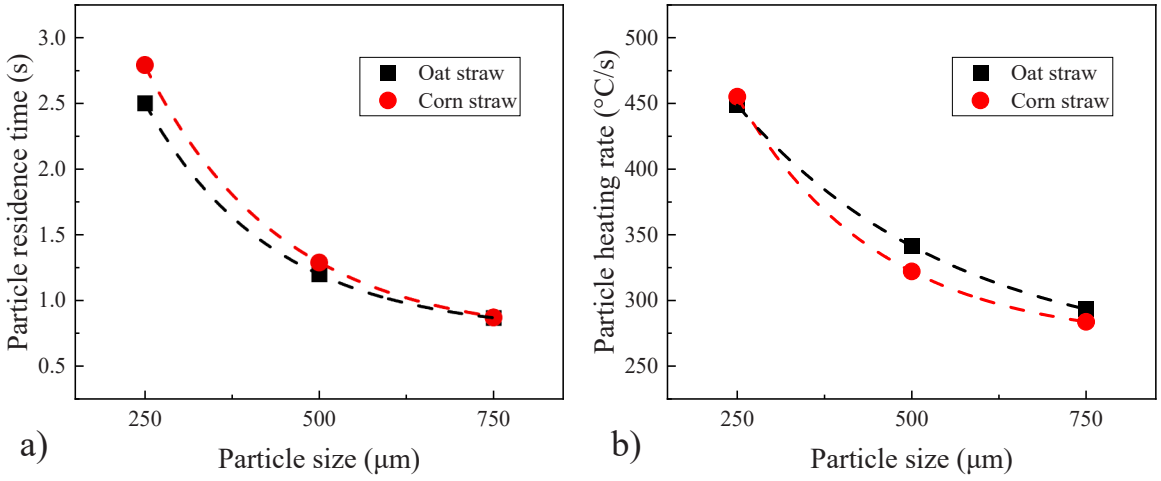

Fig. 5. Results of a) particle residence time and b) particle heating rate as a function of particle size.

particle size of 250 µm, the heating rate was approximately 450 °C/s. This value subsequently dropped to approximately 300 °C/s as the particle size increased to 750 µm. This observation could be related to heat conduction inside the particle. The Biot number (Bi) was used to investigate the heat conduction within the particles. The Biot number is a dimensionless number that characterises the influence of conduction within a solid body on convection at its surface. The results are shown in Fig. 6.

Fig. 6 shows that the Biot number increased from approximately 0.45 at a particle size of 250 µm to 0.9 at 750 µm. It can be concluded that decreasing the particle size can reduce heat conduction resistance. Small biomass particles have a large surface-area-to-volume ratios. Thus, the temperature gradient inside the particles was low, leading to fast and more uniform heating. Owing to fast heating, small particles undergo rapid thermal conversion and increased release of vapour compounds [34]. Moreover, it is noteworthy that biomass particles are weak heat conductors. A large particle size increases the resistance to heat, and during a short residence time, the particles cannot gain the appropriate temperature to begin pyrolysing [35].

There are many publications concerning the determination of particle size to facilitate bio-oil production, but most are related to fixed-bed [36,37] and fluidised bed reactors [38]. For a drop-tube reactor, Guizani et al. found that a particle size of 370 µm provides 62.4% bio-oil yield. In other studies, Ellens and Brown [12] did not observe significant

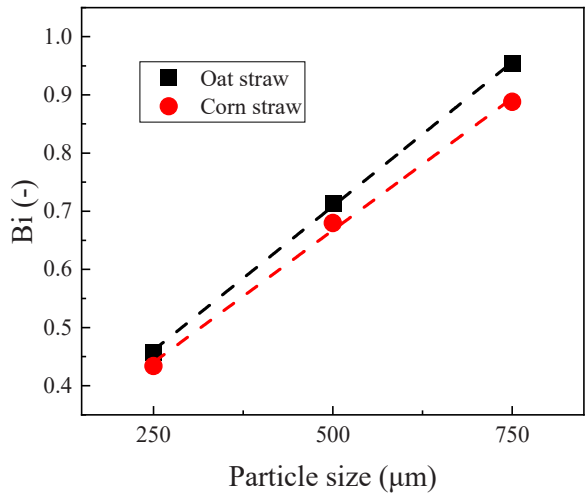

Fig. 6. Results of Biot number for both feedstocks as a function of particle size.

differences in bio-oil yield for particle sizes in the range of 200 – 600 μm. However, researchers noticed that particles larger than 1000 μm had not fully decomposed.

3.2. Impact of carrier gas flow rate

Fig. 7 presents the product yields as a function of the volume flow rate of the carrier gas (nitrogen) for oat straw and corn straw pyrolysis.

For both feedstocks, high carrier flow rates resulted in low amounts of bio-oil. The bio-oil content decreased from 51.16% and 52.09% at 3 l/min to 34.91% and 35.82% at 5 l/min for oat straw and corn straw, respectively. Additionally, the higher the flow rate, the higher was the bio-char content in the pyrolytic products. In both cases, the amount of bio-char increased from 31.91% to 54.7% for pyrolysis of oat straw and from 34.12% to 52.94% for corn straw as the flow rate increased from 3 to 5 l/min.

The results show that a high flow rate has a negative impact on fast biomass pyrolysis in a drop-tube reactor owing to a reduction in the production of bio-oil. Several factors may have affected this phenomenon. The flow rate of the carrier gas influences the residence time of the biomass particles. High flow rates caused the particles to flow fast through the reactor and did not increase the temperature to fully decompose. However, high flow rates are expected to influence the short residence time of the gaseous volatile matter. Consequently, a high flow rate can prevent thermal cracking, leading to the production of high amounts of bio-oil [39]. Another factor could be related to the reactor temperature profile and impact of the heating rate of the particles. The temperature distribution in the reactor is shown in Fig. 8. The figure is magnified 15 times in the radial direction.

As shown in Fig. 8, the temperature gradient increases when the nitrogen flow rate increases in both cases. This can be explained by the heat transfer mechanism. The heat transfer within the reactor mainly occurs via convection and radiation. As the volume flow rate increased, the heat transfer because of convection became more important, and the convective heat transfer coefficient increased [40]. Additionally, the unheated carrier gas flowed into the reactor, and some time was required to achieve temperature equilibrium with the wall temperature. At a high flow rate, the non-heated nitrogen intensified the heat exchange with the reactor walls, leading to a high temperature gradient.

A high temperature gradient affects the heat exchange between the particles and carrier gas and influences the pyrolysis process. Therefore, the particle heating rate and residence time were determined to investigate the impact of the nitrogen flow rate on these parameters. The results are shown in Fig. 9.

Fig. 9a) presents that increasing the nitrogen flow rate reduced the residence time of the particles by approximately 0.3 s. This occurred because of solid-fluid momentum exchange. The total velocity of the particle was equal to the terminal velocity and velocity of the sweeping gas. For a constant reactor geometry, a high flow rate increases the fluid velocity. From Fig. 9b), it can be observed that the higher the flow rate, the lower the heating rate. The particles mainly gain temperature because of the convective heat flow from the surrounding fluid phase [41]. The lower the local temperature of the gas, the lower is the convective heat flux to the particle surface. A decrease in the temperature of the particle surface causes a low conversion rate of the particles, leading to an increase in the bio-char yield.

The literature review relates the volume flow rate of the inert gas to the residence time of biomass particles and volatile matter. The optimal flow rate of the carrier gas depends on the reactor geometry and performance and has a wide range of values [10,42].

3.3. Impact of biomass mass load

The next parameter analysed was the biomass mass load. The results of the product yield analysis as a function of biomass feeding rate for both feedstocks are presented in Fig. 10.

These results suggested that there was no impact on the pyrolysis product concentration. At every analysed biomass feed rate, oat straw pyrolysis supplied approximately 31% of bio-char and 52% of bio-oil. A small difference was observed in corn straw pyrolysis, where the bio-char content increased from 30.75% to 35.56% as mass load of

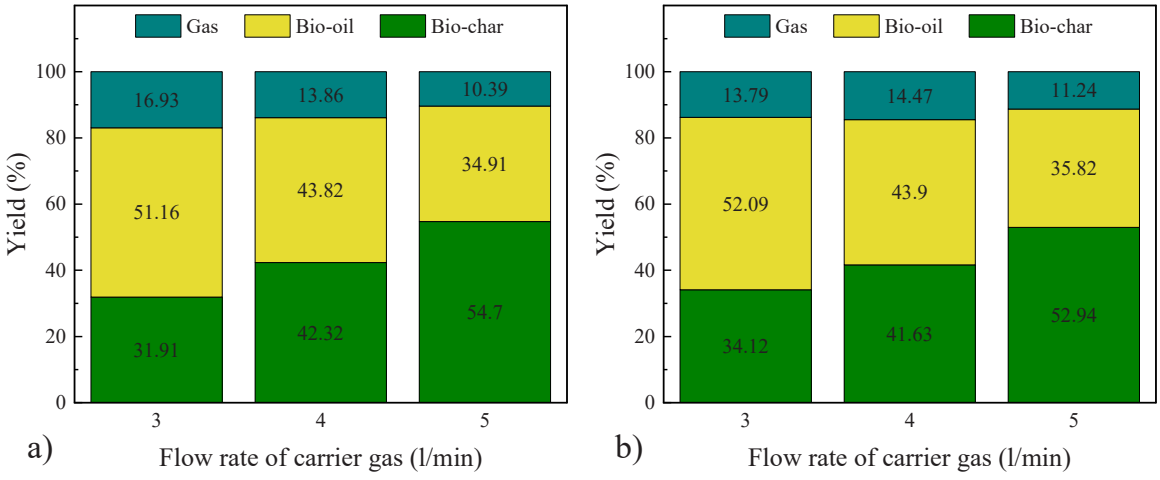

Fig. 7. Numerical results of product yields of fast pyrolysis of a) oat straw and b) corn straw as a function of carrier gas flow rate.

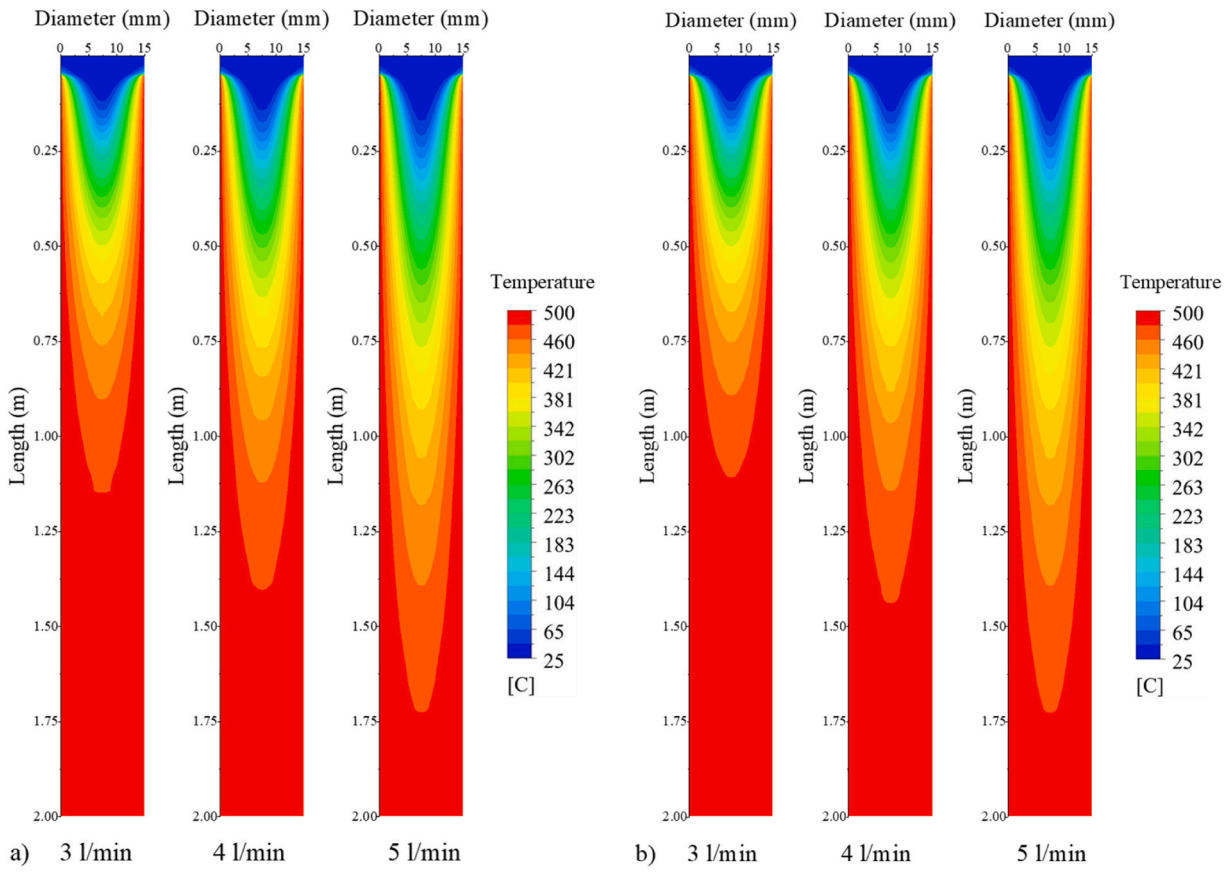

Fig. 8. Distribution of temperature for pyrolysis of a) oat straw and b) corn straw.

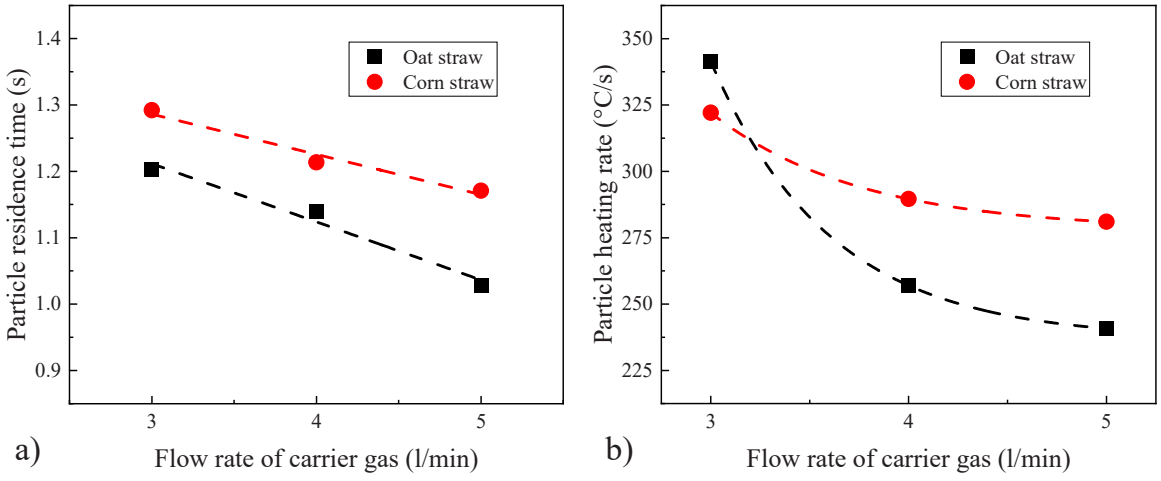

Fig. 9. Results of a) particle residence time and b) particle heating rate as a function of particle size.

biomass increased from 10 to 30 g/h. However, the yield of bio-oil remained at the same level of 51 – 52%.

The presented results are noteworthy for the following reasons. It was expected that the biomass mass load would affect the particle behaviour in the drop-tube reactor and pyrolysis process. A high mass load can lead to an increase in particle-to-particle interactions. This could affect the particle heating rate [43]. Additionally, a high feeding rate involves a high mass of biomass inside the reactor, which affects the temperature distribution owing to the heat flow from the carrier gas to the non-heated particles. In the investigated range of biomass mass loads, these effects were not significant, and perhaps a high feed rate would affect the pyrolysis process to a high degree.

3.4. Impact of temperature

Fig. 11 shows the yields of the products from oat and corn straw pyrolysis depending on the pyrolysis temperature. Bio-oil is the target product in the case of fast pyrolysis, and this result shows that increasing the pyrolysis temperature leads to a decrease in the bio-oil content [44]. The bio-oil content dropped from 51.16% to 8.47% and 52.09–9.41% in the cases of oat straw and corn straw, respectively, as the temperature increased from 500° to 700°C. Furthermore, the bio-char content

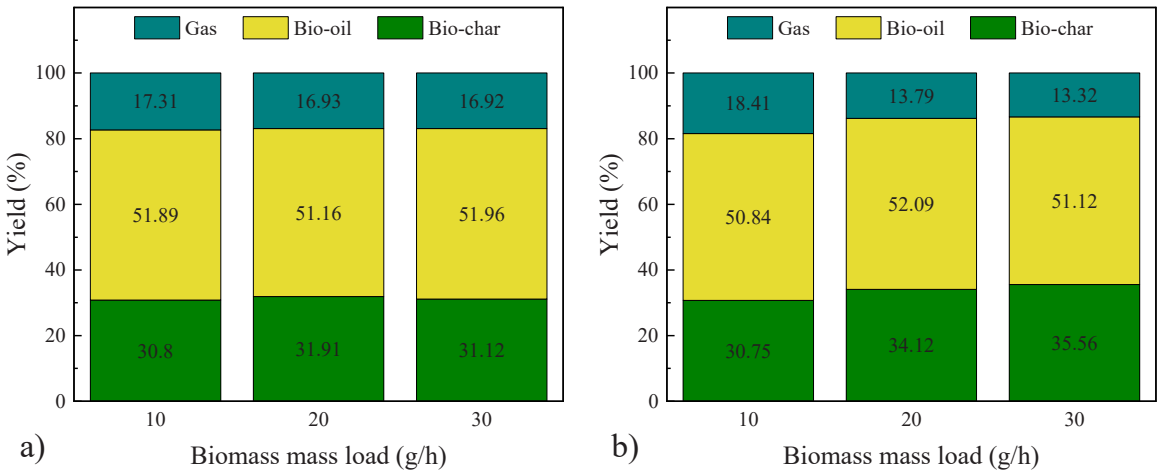

Fig. 10. Numerical results of product yields of fast pyrolysis of a) oat straw and b) corn straw as a function of biomass mass load.

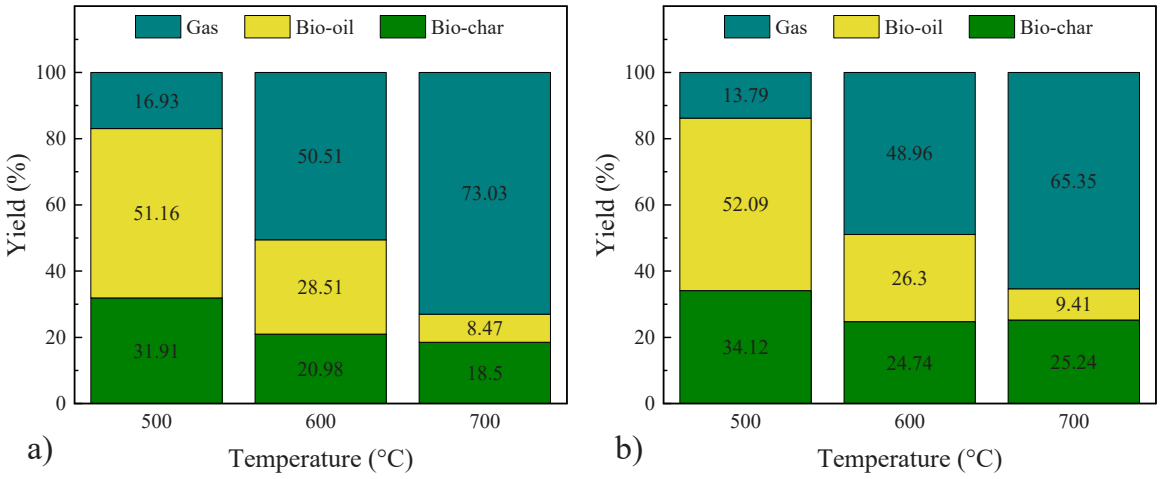

Fig. 11. Numerical results of product yields of fast pyrolysis for a) oat straw and b) corn straw as a function of pyrolysis temperature.

decreased as the temperature increased, confirming increased particle conversion. An increase in temperature favoured gas production and its content increased from 16.93% to 73.03% and 13.79–65.35% for oat straw and corn straw, respectively.

In Fig. 12, the distribution of the mass fraction of the bio-oil is presented to visualise its concentration in a drop-tube reactor. As previously mentioned, this figure was magnified 15 times in the axial direction.

From the presented graphs, it can be observed that at a high pyrolysis temperature, the highest mass fraction of bio-oil shifted toward the reactor centre. This is because of the high heating rate value at a given temperature, as shown in Fig. 13 b). Additionally, on Fig. 13 a), the particle residence time was determined.

As shown in Fig. 13 a), it can be seen that increasing the temperature did not influence the residence time of the particles. This is because of the lack of additional momentum which can be transferred to the particles. Fig. 13 b) shows that a temperature of 700 °C increased the heating rate by approximately 100 °C/s.

Fig. 12 presents that as the reactor length increased, the bio-oil mass fraction started to decrease. The following figure confirms that these effects are more significant at high temperatures. Owing to the high temperature, the biomass particle heating rate was high, and the particles started pyrolysing in the early stages of the reactor [45]. The secondary reactions of thermal cracking are influenced by high temperatures, leading to the thermal decomposition of bio-oil into lightweight gases [46]. At high temperatures, volatile matter is released early and vapours remain inside the reactor for long, enhancing the thermal cracking reactions. Low pyrolysis temperatures can be used to prevent bio-oil decomposition. Additionally, it is worth considering a short reactor or a high flow rate of the carrier gas to provide a low residence time for the bio-oil inside the heating zone.

According to [10], pyrolysis temperature is a crucial factor in bio-oil production and is the most investigated parameter. Some studies suggest that the temperature range of 450 – 550 °C provides the highest bio-oil content [42,47]. In case of drop-tube reactor, Ellens and Brown [12] proposed a temperature of 550 °C for maximisation of bio-oil production.

4. Experimental verification

The selection of the operating parameters is an iterative process that involves experiments or calculations to achieve the desired product yields or high process efficiency. Many factors influence the choice of the best parameters, such as reactor performance or feedstock characterisation. During the selection, it is noteworthy that there is no unified formula to describe the best parameters. This selection was based on the previously set targets. The presented numerical analysis can aid in determining the optimal operating conditions for maximising bio-oil production.

To confirm the numerical results, experimental verification was performed for selected parameters characterised by a high bio-oil yield.

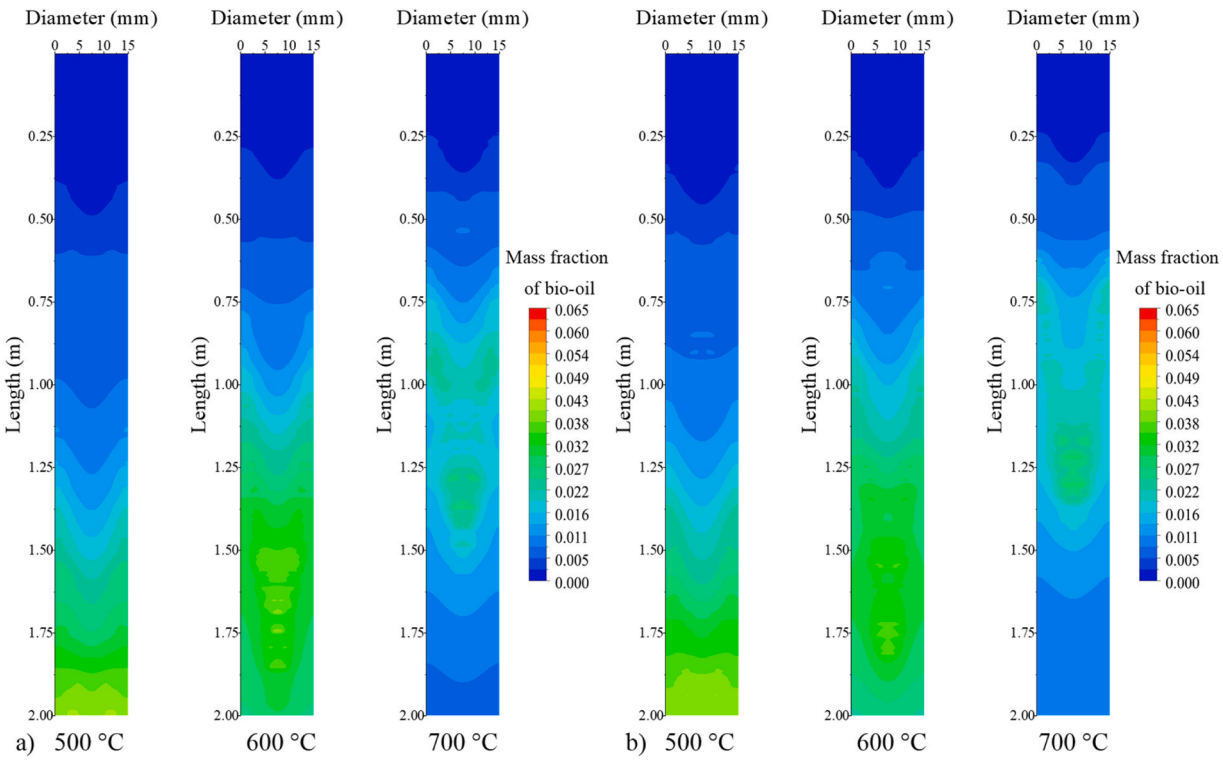

Fig. 12. Distribution of bio-oil in the drop-tube reactor for pyrolysis of a) oat straw and b) corn straw.

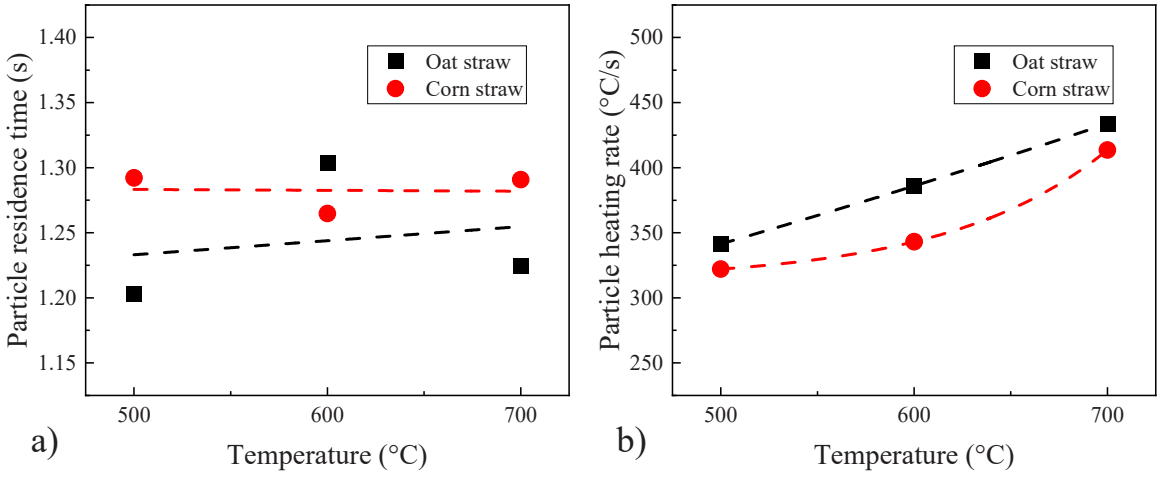

Fig. 13. Results of a) particle residence time and b) particle heating rate as a function of temperature.

Each investigation was conducted at least thrice to confirm the repeatability of the results. The error was calculated using the three-sigma rule, in which the standard deviation of the mean was estimated. The operating conditions for the reference parameters were selected. Numerical analysis showed that these parameters are promising for producing a high bio-oil yield. However, it is noteworthy that small biomass particles also provide high biomass conversion and more gas can be produced. This is important when fast pyrolysis is focused on maximising the conversion of biomass particles into vapour products [48].

A comparison of the product yields from the experiments and calculations is shown in Fig. 14. Experimental investigations confirmed the product yields obtained from numerical calculations. Under selected conditions, the experiments provided average bio-oil contents of 53.2% and 51.3% for oat straw and corn straw, respectively, and bio-char contents of 30.1% and 29.8%. It shows that under a particle size of 500 μm. it is possible to convert a large part of biomass.

The chosen reaction mechanism did not allow determination of the composition of the bio-oil based on numerical calculations. However, by making some assumptions, it was possible to estimate the carbon content in the bio-char based on numerical results [49]. This method was applied to verify the numerical results and can be useful for investigating the quality of bio-char in future studies. A detailed description of the methodology has been added in the Supplementary Material. Fig. 15 presents the carbon content in the raw material and bio-char obtained from the experiments and calculations for both feedstocks. The carbon content in the experiment was determined using a Leco analyser, as described in Section 2.1. The experimental results verified that the applied methodology could be successfully used to investigate bio-char quality in numerical studies. According to the experimental results, bio-char from oat straw pyrolysis contained 70.4% of carbon, whereas

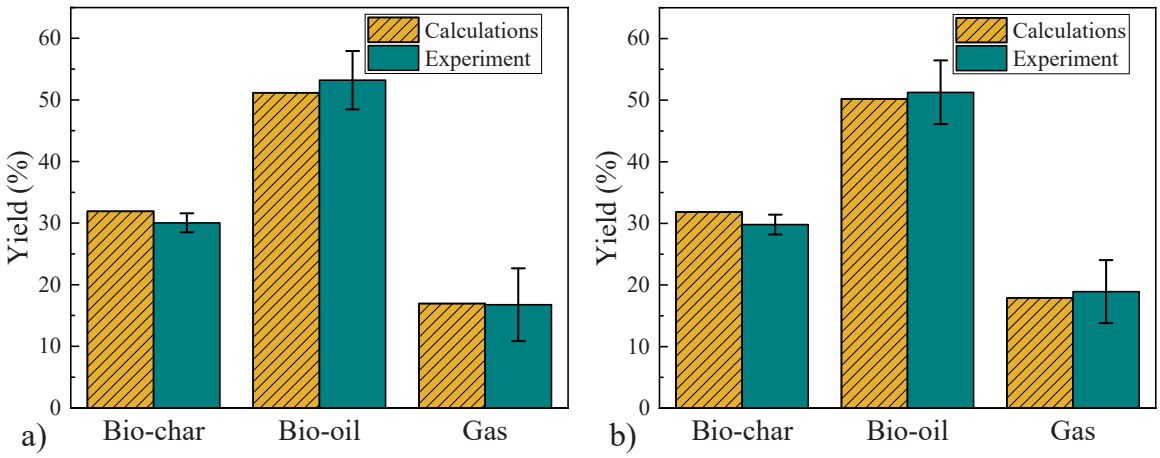

Fig. 14. Products yields from experiments and calculations obtained for pyrolysis of a) oat straw and b) corn straw.

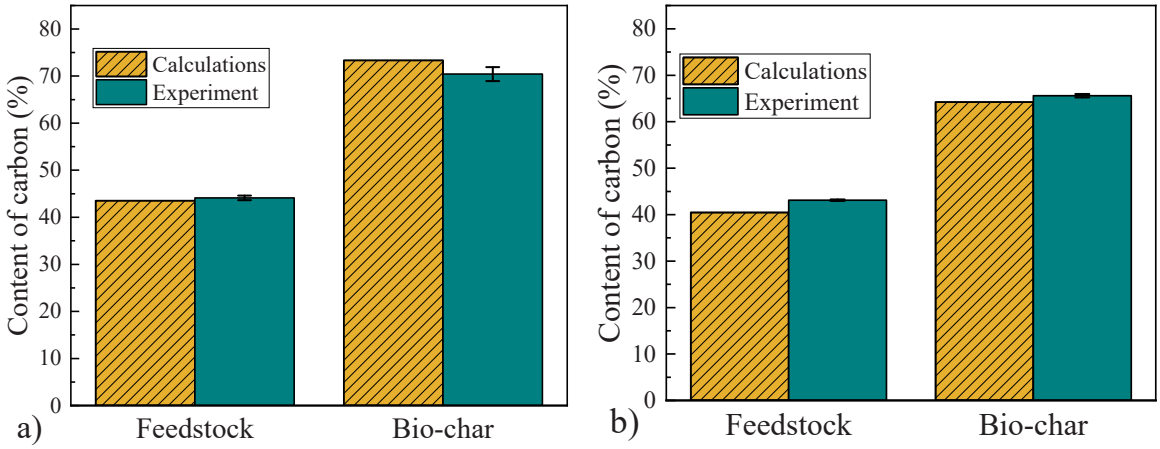

Fig. 15. Carbon content in bio-char from experiments and calculations obtained for pyrolysis of a) oat straw and b) corn straw.

calculations provided 73.3%. In the case of corn straw, the experimental measurements indicated 65.6% carbon, whereas the numerical results indicated 64.2%. Some differences may result from simplifications made during the calculation.

5. Conclusions

This study presents numerical calculations for the fast pyrolysis of agricultural biomass in a drop-tube reactor. An analysis was performed to investigate the impacts of four parameters on the production of bio-oil: temperature, particle size, carrier gas flow rate, and biomass mass load. The selected parameters with high bio-oil yields were experimentally tested. The conducted analysis allowed the following conclusions to be drawn:

- The particle size of the biomass is crucial for biomass conversion. The larger the particle size, the longer the reactor should be to provide full conversion of the feedstock. Particles with a diameter of 750 μm did not undergo pyrolysis in the given reactor geometry.
- A high volumetric nitrogen flow resulted in a temperature gradient within the reactor and reduced the degree of biomass conversion. The highest bio-oil yield was obtained at a flow rate of 3 l/min.
- The mass load of the biomass had a small impact on the yield of the pyrolysis products.
- A high pyrolysis temperature increased the degree of biomass conversion but negatively affected the bio-oil yield as a result of thermal cracking.
- The numerical results were successfully confirmed by experiments.
- The presented numerical model can be useful for the prediction of the pyrolytic yield in preliminary studies without involving many experimental investigations.

CRediT authorship contribution statement

Artur Bieniek: Conceptualization, Methodology, Software, Investigation, Data curation, Writing – original draft, Visualization. **Małgorzata Sieradzka:** Investigation, Resources, Data curation, Visualization, Writing – original draft. **Wojciech Jerzak:** Investigation, Writing – original draft, Writing – review & editing, Visualization, Supervision. **Aneta Magdziarz:** Conceptualization, Methodology, Resources, Supervision, Writing – review & editing, Project administration, Funding acquisition.

Declaration of Competing Interest

The authors declare that they have no known competing financial interests or personal relationships that could have appeared to influence the work reported in this paper.

Data Availability

Data will be made available on request.

Acknowledgement

This research was funded in whole by the National Science Centre of Poland [grant no. 2020/39/B/ST8/00883].

Appendix A. Supporting information

Supplementary data associated with this article can be found in the online version at doi:10.1016/j.jaap.2023.106241.

References

[1] D.A. Akinpelu, O.A. Adekoya, P.O. Oladoye, C.C. Ogbaga, J.A. Okolie, Machine learning applications in biomass pyrolysis: from biorefinery to end-of-life product management, Digit. Chem. Eng. 8 (2023), 100103, https://doi.org/10.1016/j.dche.2023.100103.
[2] Z. Kaczor, Z. Buliński, S. Werle, Modelling approaches to waste biomass pyrolysis: a review, Renew. Energy 159 (2020) 427–443, https://doi.org/10.1016/j.renene.2020.05.110.
[3] Q. Bu, J. Cai, Y. Liu, M. Cao, L. Dong, R. Ruan, H. Mao, The effect of fuzzy PID temperature control on thermal behavior analysis and kinetics study of biomass microwave pyrolysis, J. Anal. Appl. Pyrolysis 158 (2021), 105176, https://doi.org/10.1016/j.jaap.2021.105176.
[4] P. Basu, Biomass gasification, pyrolysis and torrefaction, Pract. Des. Theory, Elsevier Inc. (2013), https://doi.org/10.1016/C2011-0-07564-6.
[5] S. Sobek, S. Werle, Solar pyrolysis of waste biomass: Part 1 reactor design, Renew. Energy 143 (2019) 1939–1948, https://doi.org/10.1016/j.renene.2019.06.011.
[6] D.O. Usino, P. Ylitervo, A. Moreno, M.H. Sipponen, T. Richards, Primary interactions of biomass components during fast pyrolysis, J. Anal. Appl. Pyrolysis 159 (2021), 105297, https://doi.org/10.1016/j.jaap.2021.105297.
[7] B. Li, M. Song, X. Xie, J. Wei, D. Xu, K. Ding, Y. Huang, S. Zhang, X. Hu, S. Zhang, D. Liu, Oxidative fast pyrolysis of biomass in a quartz tube fluidized bed reactor: Effect of oxygen equivalence ratio, Energy 270 (2023), 126987, https://doi.org/10.1016/j.energy.2023.126987.
[8] W.M. Lewandowski, K. Januszewicz, W. Kosakowski, Efficiency and proportions of waste tyre pyrolysis products depending on the reactor type—A review, J. Anal. Appl. Pyrolysis 140 (2019) 25–53, https://doi.org/10.1016/j.jaap.2019.03.018.
[9] D. Wang, Z. Chen, C. Li, D. Wang, Y. Li, H. Yang, Z. Liu, J. Yu, S. Gao, High-quality tar production from coal in an integrated reactor: Rapid pyrolysis in a drop tube and downstream volatiles upgrading over char in a moving bed, Fuel 285 (2021), 119156, https://doi.org/10.1016/j.fuel.2020.119156.
[10] R.E. Guedes, A.S. Luna, A.R. Torres, Operating parameters for bio-oil production in biomass pyrolysis: A review, J. Anal. Appl. Pyrolysis 129 (2018) 134–149, https://doi.org/10.1016/j.jaap.2017.11.019.
[11] C. Guizani, S. Valin, J. Billaud, M. Peyrot, S. Salvador, Biomass fast pyrolysis in a drop tube reactor for bio oil production: Experiments and modeling, Fuel 207 (2017) 71–84, https://doi.org/10.1016/j.fuel.2017.06.068.
[12] C.J. Ellens, R.C. Brown, Optimization of a free-fall reactor for the production of fast pyrolysis bio-oil, Bioresour. Technol. 103 (2012) 374–380, https://doi.org/10.1016/j.biortech.2011.09.087.
[13] A. Bieniek, W. Jerzak, M. Gajek, A. Magdziarz, Numerical investigations of biomass pyrolysis with partial oxidation in a drop tube reactor, J. Clean. Prod. 401 (2023), 136774, https://doi.org/10.1016/j.jclepro.2023.136774.
[14] P. Gable, R.C. Brown, Effect of biomass heating time on bio-oil yields in a free fall fast pyrolysis reactor, Fuel 166 (2016) 361–366, https://doi.org/10.1016/j.fuel.2015.10.073.
[15] L. Wei, S. Xu, L. Zhang, H. Zhang, C. Liu, H. Zhu, S. Liu, Characteristics of fast pyrolysis of biomass in a free fall reactor, Fuel Process. Technol. 87 (2006) 863–871, https://doi.org/10.1016/j.fuproc.2006.06.002.
[16] A. Pattiya, S. Sukkasi, V. Goodwin, Fast pyrolysis of sugarcane and cassava residues in a free-fall reactor, Energy 44 (2012) 1067–1077, https://doi.org/10.1016/j.energy.2012.04.035.
[17] R.S. Miller, J. Bellan, A generalized biomass pyrolysis model based on superimposed cellulose, hemicellulose and lignin kinetics, Combust. Sci. Technol. 126 (1997) 97–137, https://doi.org/10.1080/00102209708935670.
[18] T. Ding, S. Li, J. Xie, W. Song, J. Yao, W. Lin, Rapid Pyrolysis of Wheat Straw in a Bench-Scale Circulating Fluidized-Bed Downer, React., Chem. Eng. Technol. 35 (2012) 2170–2176, https://doi.org/10.1002/CEAT.201200140.
[19] W. Cao, J. Li, T. Martí-Rosselló, X. Zhang, Experimental study on the ignition characteristics of cellulose, hemicellulose, lignin and their mixtures, J. Energy Inst. 92 (2019) 1303–1312, https://doi.org/10.1016/j.joei.2018.10.004.
[20] Q. Xue, D. Dalluge, T.J. Heindel, R.O. Fox, R.C. Brown, Experimental validation and CFD modeling study of biomass fast pyrolysis in fluidized-bed reactors, Fuel 97 (2012) 757–769, https://doi.org/10.1016/J.FUEL.2012.02.065.
[21] S. Aramideh, Q. Xiong, S.-C. Kong, R.C. Brown, Numerical simulation of biomass fast pyrolysis in an auger reactor, Fuel 156 (2015) 234–242, https://doi.org/10.1016/j.fuel.2015.04.038.
[22] Q. Xue, T.J. Heindel, R.O. Fox, A CFD model for biomass fast pyrolysis in fluidized-bed reactors, Chem. Eng. Sci. 66 (2011) 2440–2452, https://doi.org/10.1016/J.CES.2011.03.010.
[23] R. Kong, D. Bi, D. Yao, Y. Zhang, J. He, J. Liu, CFD-DEM study of a V-shaped Down-tube pyrolysis Reactor: Flow and heat transfer between heat carrier and biomass, Appl. Therm. Eng. 207 (2022), 118179, https://doi.org/10.1016/j.applthermaleng.2022.118179.
[24] Y. Tobo, A. Lotfi, L.D. Virla, N. Mahinpey, Fast pyrolysis multiphase CFD-kinetics model in a drop tube reactor, Fuel 340 (2023), 127524, https://doi.org/10.1016/j.fuel.2023.127524.
[25] P.J.V. Soest, Use of Detergents in the Analysis of Fibrous Feeds. II. A Rapid Method for the Determination of Fiber and Lignin, J. Assoc. Off. Anal. Chem. 73 (1990) 491–497, https://doi.org/10.1093/jaoac/73.4.491.
[26] P. Kosky, R. Balmer, W. Keat, G. Wise, Mechanical Engineering, in: P. Kosky, R. Balmer, W. Keat, G. Wise (Eds.), Exploring Engineering, Third edition.,, Academic Press, Boston, 2013, pp. 259–281, https://doi.org/10.1016/B978-0-12-415891-7.00012-1.
[27] A.H. Mahmoudi, M. Markovic, B. Peters, G. Brem, An experimental and numerical study of wood combustion in a fixed bed using Euler–Lagrange approach (XDEM, Fuel 150 (2015) 573–582, https://doi.org/10.1016/j.fuel.2015.02.008.
[28] ANSYS FLUENT 12.0 Theory Guide,. https://www.afs.enea.it/project/neptunius/docs/fluent/html/th/main_pre.htm (accessed September 8, 2022).
[29] S.A. Morsi, A.J. Alexander, An investigation of particle trajectories in two-phase flow systems, J. Fluid Mech. 55 (1972) 193–208, https://doi.org/10.1017/S0022112072001806.
[30] W.E. Ranz, W.R. Marshall, Evaporation from drops: Part II, Chem. Eng. Prog. 48 (1952) 173–180.
[31] H.A. McGee, Molecular engineering, McGraw Hill, New York, 1991.
[32] H. Ansarifar, M. Shams, Numerical simulation of hydrogen production by gasification of large biomass particles in high temperature fluidized bed reactor, Int. J. Hydrog. Energy 43 (2018) 5314–5330, https://doi.org/10.1016/j.ijhydene.2017.10.132.
[33] G. Bagheri, C. Bonadonna, - Aerodynamics of Volcanic Particles: Characterization of Size, Shape, and Settling Velocity, in: S. Mackie, K. Cashman, H. Ricketts, A. Rust, M. Watson (Eds.), Volcanic Ash, Elsevier, 2016, pp. 39–52, https://doi.org/10.1016/B978-0-08-100405-0.00005-7.
[34] M.-S. Safdari, E. Amini, D.R. Weise, T.H. Fletcher, Heating rate and temperature effects on pyrolysis products from live wildland fuels, Fuel 242 (2019) 295–304, https://doi.org/10.1016/j.fuel.2019.01.040.
[35] J. Akhtar, N.Saidina Amin, A review on operating parameters for optimum liquid oil yield in biomass pyrolysis, Renew. Sustain. Energy Rev. 16 (2012) 5101–5109, https://doi.org/10.1016/j.rser.2012.05.033.
[36] R. Garg, N. Anand, D. Kumar, Pyrolysis of babool seeds (Acacia nilotica) in a fixed bed reactor and bio-oil characterization, Renew. Energy 96 (2016) 167–171, https://doi.org/10.1016/j.renene.2016.04.059.
[37] Ö. Onay, S.H. Beis, Ö.M. Koçkar, Fast pyrolysis of rape seed in a well-swept fixed-bed reactor, J. Anal. Appl. Pyrolysis 58– 59 (2001) 995–1007, https://doi.org/10.1016/S0165-2370(00)00133-9.
[38] B.-S. Kang, K.H. Lee, H.J. Park, Y.-K. Park, J.-S. Kim, Fast pyrolysis of radiata pine in a bench scale plant with a fluidized bed: Influence of a char separation system and reaction conditions on the production of bio-oil, J. Anal. Appl. Pyrolysis 76 (2006) 32–37, https://doi.org/10.1016/j.jaap.2005.06.012.
[39] D.Ab Taleb, H.A. Hamid, R.R.R. Deris, M. Zulkifli, N.A. Khalil, A.N. Ahmad Yahaya, Insights into pyrolysis of waste tire in fixed bed reactor: Thermal behavior, Mater. Today.: Proc. 31 (2020) 178–186, https://doi.org/10.1016/j.matpr.2020.01.569.
[40] Y.A. Çengel, A.J. Ghajar, Heat and Mass Transfer: Fundamentals & Applications, McGraw Hill Education, 2015.
[41] A.V. Bridgwater, Review of fast pyrolysis of biomass and product upgrading, Biomass-.-. Bioenergy 38 (2012) 68–94, https://doi.org/10.1016/j.biombioe.2011.01.048.
[42] M. Tripathi, J.N. Sahu, P. Ganesan, Effect of process parameters on production of biochar from biomass waste through pyrolysis: A review, Renew. Sustain. Energy Rev. 55 (2016) 467–481, https://doi.org/10.1016/J.RSER.2015.10.122.
[43] K.M. Qureshi, A.N.K. Lup, S. Khan, F. Abnisa, W.M.A.W. Daud, Effect of temperature and feed rate on pyrolysis oil produced via helical screw fluidized bed reactor, Korean J. Chem. Eng. 38 (2021) 1797–1809, https://doi.org/10.1007/s11814-021-0842-0.
[44] J.L. Klinger, T.L. Westover, R.M. Emerson, C.L. Williams, S. Hernandez, G. D. Monson, J.C. Ryan, Effect of biomass type, heating rate, and sample size on microwave-enhanced fast pyrolysis product yields and qualities, Appl. Energy 228 (2018) 535–545, https://doi.org/10.1016/J.APENERGY.2018.06.107.
[45] R. Mehrabian, R. Scharler, I. Obernberger, Effects of pyrolysis conditions on the heating rate in biomass particles and applicability of TGA kinetic parameters in particle thermal conversion modelling, Fuel 93 (2012) 567–575, https://doi.org/10.1016/j.fuel.2011.09.054.
[46] G. Qi, Z. Wang, S. Zhang, Y. Dong, J. Guan, P. Dong, Numerical simulation on biomass-pyrolysis and thermal cracking of condensable volatile component, Int. J. Hydrog. Energy 45 (2020) 12283–12297, https://doi.org/10.1016/j.ijhydene.2020.02.199.
[47] P. Das, A. Ganesh, Bio-oil from pyrolysis of cashew nut shell—a near fuel, Biomass-.-. Bioenergy 25 (2003) 113–117, https://doi.org/10.1016/S0961-9534(02)00182-4.
[48] M. Sharifzadeh, L. Wang, N. Shah, Integrated biorefineries: CO_2 utilization for maximum biomass conversion, Renew. Sustain. Energy Rev. 47 (2015) 151–161, https://doi.org/10.1016/j.rser.2015.03.001.
[49] O.A. Oyedeji, M. Brennan Pecha, C.E.A. Finney, C.A. Peterson, R.G. Smith, Z. G. Mills, X. Gao, M. Shahnam, W.A. Rogers, P.N. Ciesielski, R.C. Brown, J. E. Parks II, CFD–DEM modeling of autothermal pyrolysis of corn stover with a coupled particle- and reactor-scale framework, Chem. Eng. J. 446 (2022), 136920, https://doi.org/10.1016/j.cej.2022.136920.